JMEPEG (2011) 20:517–521
DOI: 10.1007/s11665-011-9853-z

1059-9495/$19.00

Property of Amorphous/Nanocrystalline Hybrid Wires of TiNi-Base Shape Memory Alloys

Koichi Tsuchiya and Tadahiro Koike

(Submitted June 16, 2010)

The microstructures and mechanical properties of amorphous/nanocrystalline hybrid TiNi wires produced by severe cold drawing were investigated. Annealed wires of Ti-50.9 mol%Ni and Ti-41 mol%Ni-8.5 mol%Cu were subjected to severe cold drawing of 50-70% reduction. The as-drawn TiNi wires were composed of the mixture of amorphous phase and predominantly B2 nanocrystalline phase. Young's modulus increased with the drawing reduction which can be attributed to the increase in the amount of amorphous phase. For the binary TiNi wires, the volume fraction of amorphous phase was estimated to be about 60% from Young's modulus and electrical resistivity. The wires drawn over 60% exhibited peculiar large linear elastic strain which is quite different from superelasticity. Aging at 573 K led to an increase in tensile elongation as well as in the recoverable strain. The amorphization by cold drawing was also confirmed for Ti-41 mol%Ni-8.5 mol%Cu in 62% drawn wires.

Keywords amorphous, nanocrystalline, shape memory alloy, superelasticity

1. Introduction

Plastic deformation has been used as one of the practical means to control the microstructures and to stabilize shape memory effect and superelasticity in TiNi shape memory alloys for many years. Recently, there have been an increasing interest on amorphous TiNi processed by means of severe plastic deformation such as cold rolling (Ref 1) and high-pressure torsion deformation (Ref 2). Nanocrystalline TiNi can be obtained through ''devitrification'' of amorphous TiNi by postdeformation heat treatment (Ref 3).

The obtained nanocrystalline or ultrafine grains are beneficial to increase the yield stress of the material; meanwhile, both thermal- or stress-induced martensitic transformation can be strongly influenced by the grain size if it is below 100 nm (Ref 4). The interplay between these two effects has not been clarified yet. The effect of the grain refinement to nanoscale on martensitic transformation is fourfold: (1) suppress the forward martensitic transformation, (2) increases the transformation temperature width ($\Delta M = M_s - M_f$), (3) the reverse transformation behavior is less affected, and (4) stabilize R phase (Ref 5).

This article describes that the amorphous/nanocrystalline hybrid wires can be produced by severe cold drawing over 50% area reduction. These amorphous/nanocrystalline TiNi was shown to exhibit superior properties, such as the higher elastic modulus (Ref 6). Effect of cold drawing in Ti-Ni-Cu is also described.

2. Experimental Procedures

Annealed wires of Ti-50.9 mol%Ni and Ti-41 mol%Ni-8.5 mol%Cu were cold-drawn to the areal reduction of 50-70% using diamond dies without intermitting annealing. Details of analysis method used to characterize the microstructures of binary TiNi wires were described elsewhere (Ref 6).

For the characterization of Ti-41 mol%Ni-8.5 mol%Cu, x-ray diffractometry (XRD) was conducted using Cu K_α radiation generated at 40 kV-300 mA. Samples for transmission electron microscopy (TEM) were prepared by electrochemical polishing. A small piece of the wire was mechanically thinned down to the thickness of 0.2 mm from both side, and was mounted onto a Pt-grid. Electro-chemical polishing was done on Tenupol-6 with H_2SO_4/methanol at 253 K. Microstructures were observed on TEM operated at 200 kV.

3. Results and Discussion

3.1 Structures and Properties of Ti-50.9Ni

Figure 1(a) is the XRD patterns of Ti-50.9Ni wires for different drawing reductions. It is apparent that the cold drawing leads to the marked decrease in the peak intensity and to the peak broadening. The crystallite size was evaluated using the Scherrer equation and plotted as a function of true strain in

This article is an invited paper selected from presentations at Shape Memory and Superelastic Technologies 2010, held May 16-20, 2010, in Pacific Grove, California, and has been expanded from the original presentation.

Koichi Tsuchiya, Hybrid Materials Center, National Institute for Materials Science, Department of Pure and Applied Sciences, University of Tsukuba, Sengen 1-2-1, Tsukuba, Ibaraki 305-0047, Japan; and **Tadahiro Koike**, Asahi Intecc, Co., Ltd, Izumi, Osaka, Japan. Contact e-mails: tsuchiya.koichi@nims.go.jp and tadahiro.koike@asahi-intecc.com.

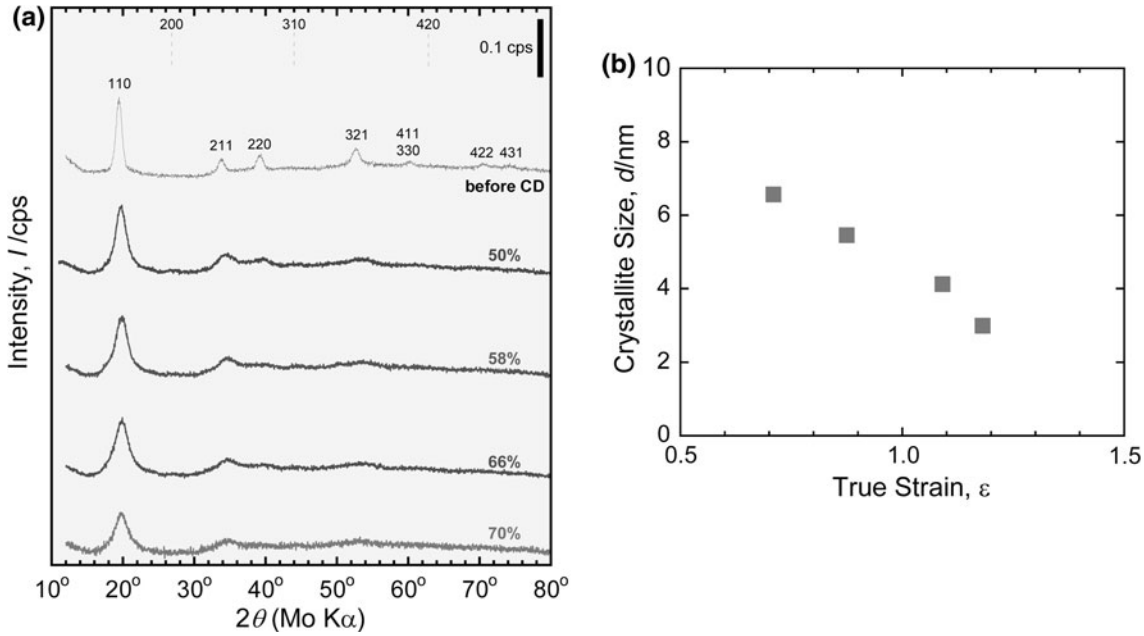

Fig. 1 (a) X-ray diffraction profiles of Ti-50.9Ni wires before and after cold drawing. (b) Crystallite size as a function of true strain

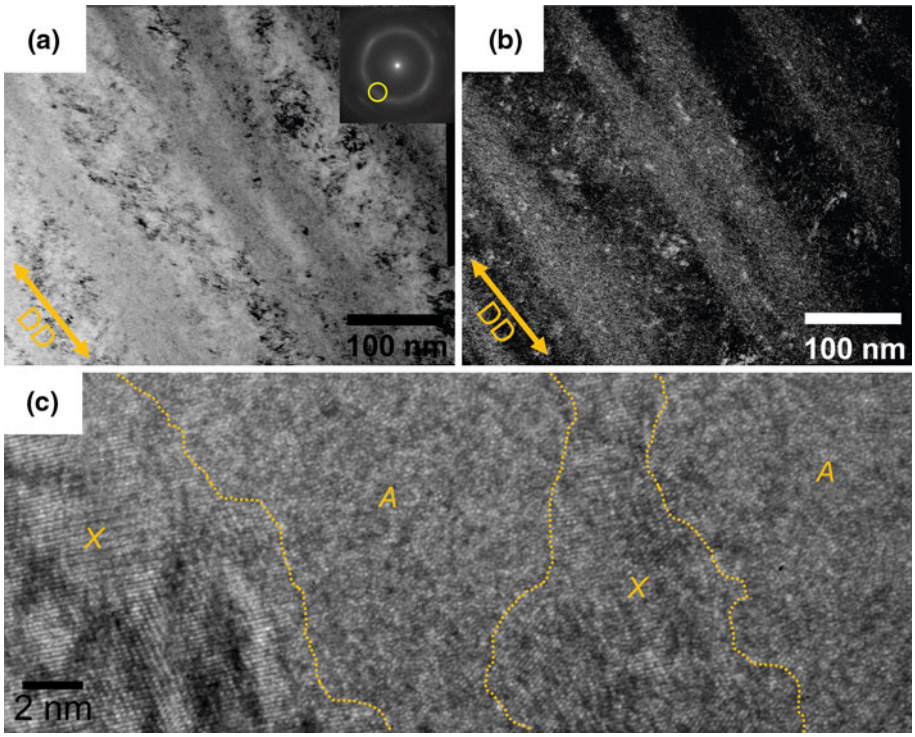

Fig. 2 TEM micrographs of Ti-50.9 mol%Ni wire after 70% cold drawing. (a) Bright field image, (b) dark field image, and (c) high-resolution image

Fig. 1(b). The crystallite size linearly decrease with the true strain and reaches to about 3 nm after 70% reduction. Figure 2 is TEM bright field (BF) image (a) and dark field (DF) image (b) of the 70% drawn wire. Drawing direction is shown by the arrows. Selected area diffraction pattern (SADP) shown as the inset of Fig. 2(b) exhibits a halo ring with the radius corresponding to the *d*-spacing of 110 plane of the B2 phase, indicating the presence of amorphous phase. Layered structures parallel to the drawing direction are apparent in the micrographs. The DF image (Fig. 2b) was obtained from a part of the hallo ring in the SADP, and supports that, in the gray layers marked as "a" in the BF image and brighter layer in the DF image, amorphous is the predominant phase with some nanocrystalline B2 phase. Meanwhile the layers, marked as "c," are in B2 nanocrystalline state. Figure 2(c) is the high-resolution TEM image of the different area of the sample. The areas denoted as "*A*" are a part of the amorphous layer similar to those marked as "a" in Fig. 2(a) and (b). They are separated

by the debris crystalline, which shows clear lattice fringes. The interfaces between the crystalline and the amorphous, delineated by the broken lines, are very irregular and not well-defined. The amorphous area contained some indication of the medium range order (MRO) clusters as seen in the amorphous phase processed by HPT (Ref 7), which may correspond to the bright speckle contrast in Fig. 2(b).

Figure 3 shows the tensile stress-strain curves of the as-drawn Ti-50.9 mol%Ni wires (Ref 6). The curve for a wire showing conventional superelasticity is also indicated for comparison. It is apparent that the cold-drawn wires possess very high-tensile strength exceeding 2 GPa. The tensile elongation decreases with increasing reduction in area. It is about 8% for 50% drawn wires and about 4% in 70% drawn one, which is remarkably large for amorphous containing material. Also, it should be emphasized that the initial slope of the stress-strain curves depends strongly on the reduction. Young's modulus, E, was evaluated from the slope of the initial part of the curves and is plotted as the inset in Fig. 4. The values

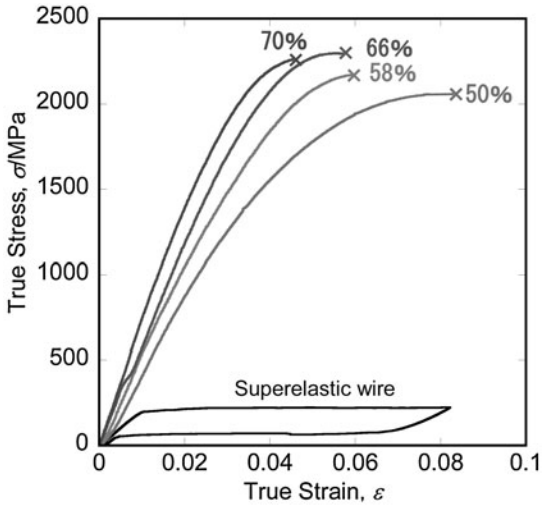

Fig. 3 Tensile stress-strain curves of as-drawn Ti-50.9Ni wires with different drawing reductions

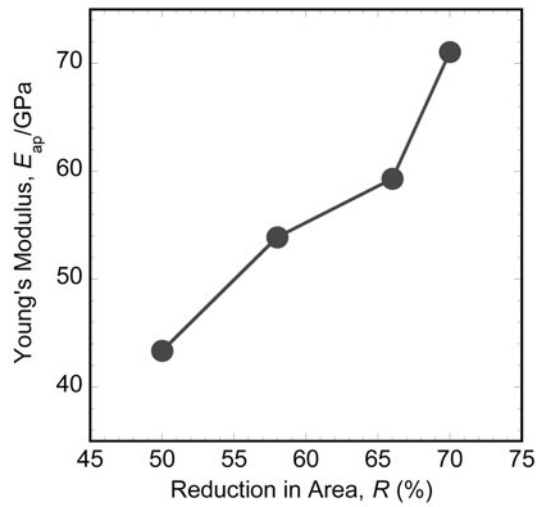

Fig. 4 Young's modulus of Ti-50.9Ni wires as a function of drawing reductions

change from 43 GPa in the 50% drawn wire to 71 GPa in the 70% drawn one. In a coarse-grained TiNi, Young's modulus was reported to be 30 GPa for the B2 phase and 18 GPa for the B19′ martensite phase (Ref 8). For amorphous thin film of Ti-47.5 mol%Ni and -52.7 mol%Ni, the value of about 93 GPa is reported (Ref 9). Thus, the Young's modulus of the amorphous/nanocrystalline wires lies between those for the crystalline TiNi and amorphous TiNi, although the tensile elongation of the wires is much larger than that of the amorphous films (~1%).

It can be inferred that the observed change in Young's modulus is due to the increase in the fraction of amorphous phase. TEM observations revealed that the as-drawn wires are composed of fibrous mixture of amorphous phase and B2 nanocrystalline phase. Using the law of mixture (the Voigt approximation), the volume fraction of amorphous phase can be estimated by using the following equation.

$$E = V_f^{B2} E_{B2} + V_f^{am} E_{am}, \quad \text{(Eq 1)}$$

where V_f and E are the volume fraction and Young's modulus, B2 and am denote the B2 phase and amorphous phase, respectively. E_{B2} = 30 GPa and E_{am} = 94 GPa are assumed. The results of estimation are shown in Fig. 5. After 50% reduction, the volume fraction was estimated to be 21% and it increased to 64.5% after 70% reduction. The volume fraction of amorphous phase was also estimated from the electrical resistivity measurements The equation similar to Eq 1 also holds for the resistivity at 5 K of the amorphous/nanocrystalline wires (Ref 10)

$$\rho = V_f^{B2} \rho_{B2} + V_f^{am} \rho_{am}, \quad \text{(Eq 2)}$$

where ρ_{B2} and ρ_{am} are the resistivity of B2 phase and amorphous phase, respectively. For the B2 phase, the value for the alloy with same composition is not available and 1.4 μΩm measured for Ti-52Ni (Ref 11) was used. For amorphous phase, 2.5 μΩm measured for RS ribbon (Ref 12) was used. The results are also plotted in Fig. 5. The V_f^{am} estimated from the resistivity in 50 and 70% drawn wires are 15 and 54%, and thus appears lower but is in good agreement with those estimated from Young's modulus.

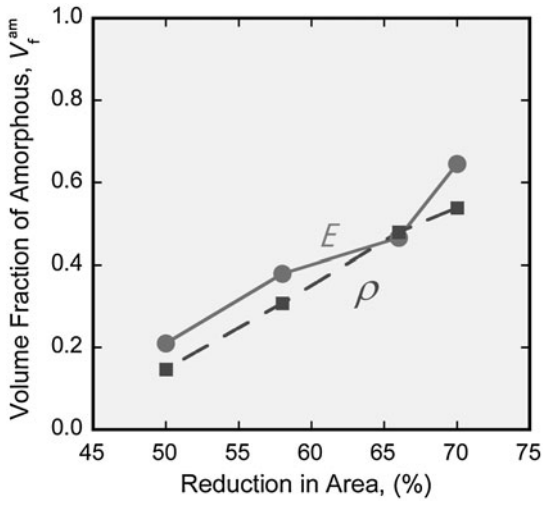

Fig. 5 Volume fraction of amorphous phase estimated from Young's modulus (circle) and electrical resistivity (square) as a function of drawing reduction

Figure 6(a) and (b) shows an example of cyclic stress-strain curve obtained for the 50 and 70% drawn wires, respectively. The 50% drawn wire exhibits stress-strain curves with large hysteresis which suggests the contribution of superelasticity. Meanwhile, the 70% drawn wire exhibits linear elastic behavior, which is very different from the conventional superelasticity in the well-annealed wires. Figure 7(a) and (b) show the stress-strain curves of the 50 and 70% drawn wires after aging at 573 K for 3.6 ks. For the 50% drawn wire, the aging bring about the superelastic plateau and enhances the hysteresis while for the 70% drawn wire, hysteresis is still very small and tensile strength and elongation increased. Effect of aging at higher temperatures led to the decrease in tensile strength and Young's modulus (Ref 5). The mechanism of the peculiar pseudoelastic recovery is not clear at this point. It cannot be the microtwinning of the (001) deformation twins of martensite phase (Ref 13) since both the x-ray diffraction and TEM observations support that the dominant phase is the amorphous or B2 nanocrystalline phase. It could be due to combined effect of superelastic deformation of nano-B2 grains and elastic deformation of amorphous phase. In situ XRD study is needed to clarify the mechanism.

3.2 Structures and Properties of Cold-Drawn Ti-41Ni-8.5Cu

X-ray diffraction and TEM observations revealed that the as-annealed wire composed of a predominant B19′ monoclinic martensite phase and a small amount of B19 orthorhombic martensite. X-ray diffraction patterns of as-drawn wires exhibited marked peak broadening, suggesting significant grain refinement took place by the drawing process. The crystallite size in 62% drawn wires were about 18 nm. Figure 8(a) is the TEM BF image and SADP (inset) of Ti-41Ni-8.5Cu before the drawing. The grain size (or martensite plate size) was several hundred nanometer and contained a high density of internal twins. Figure 8(b) shows the microstructures after drawing (62% reduction). The SADP indicates halo ring pattern overlapping with the Debye rings from B2 and B19′ martensite

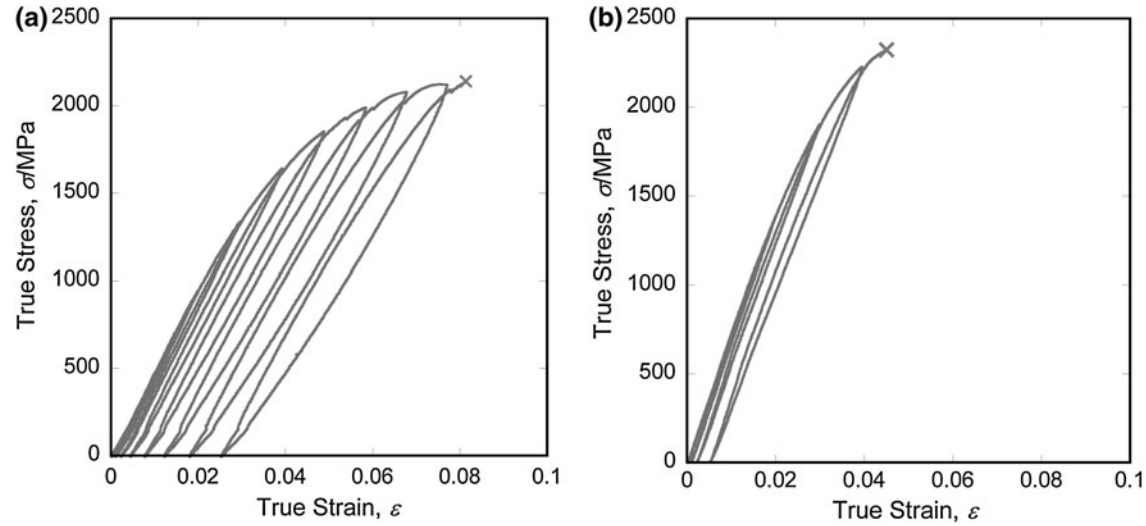

Fig. 6 Cyclic stress-strain curves of as-drawn Ti-50.9Ni wires. (a) 50% reduction and (b) 70% reduction

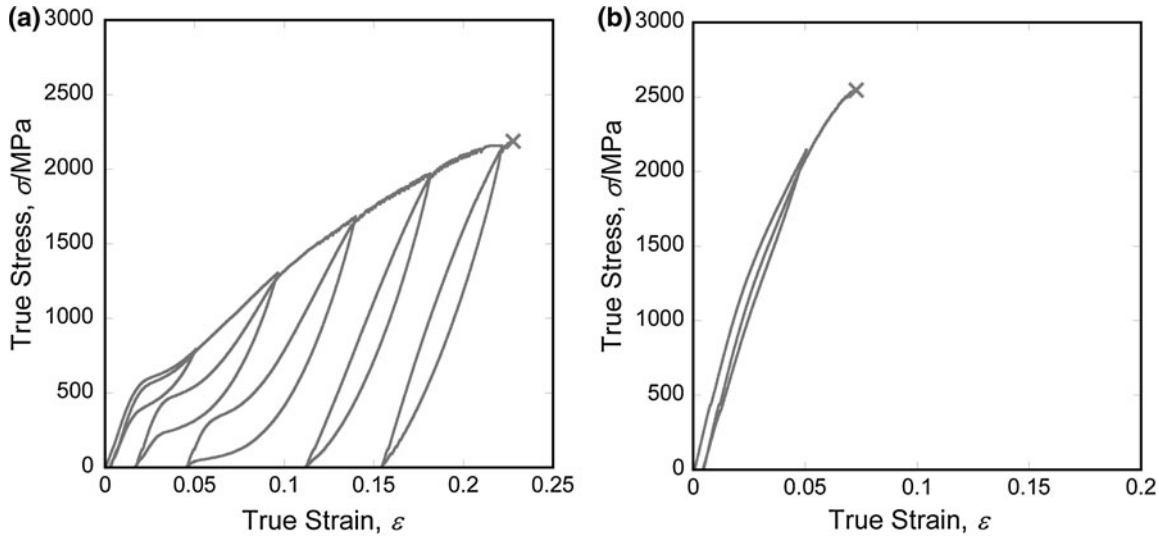

Fig. 7 Cyclic stress-strain curves of Ti-50.9Ni wires after aging at 573 K for 3.6 ks. (a) 50% reduction and (b) 70% reduction

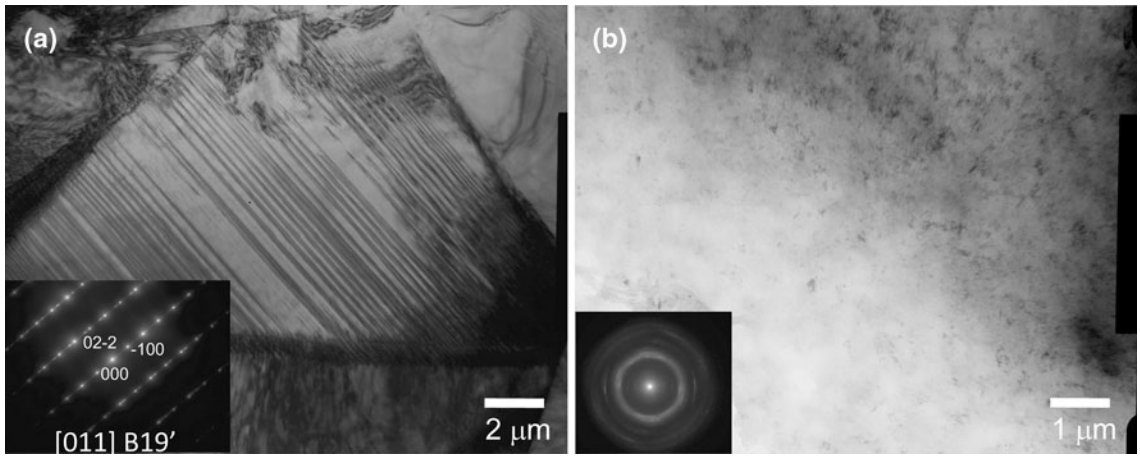

Fig. 8 TEM micrographs of Ti-41Ni-8.5Cu wires. (a) Before drawing and (b) after 62% drawing

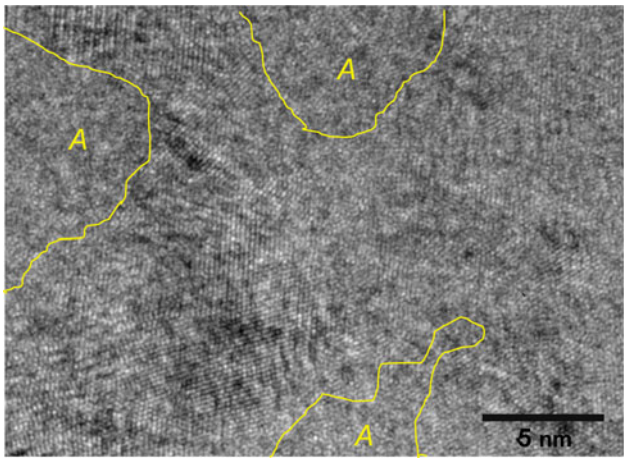

Fig. 9 High-resolution TEM micrographs of Ti-41Ni-8.5Cu wires after 62% drawing. "*A*" denotes the amorphous area

phase. The radius of halo ring is close to $|g_{110}|$. The size of dark patch like contrast agrees with the crystallite size obtained from XRD. Presence of amorphous phase was also confirmed by high-resolution TEM as shown in Fig. 9. It is seen that the sample is composed of nanocrystalline of B2 and amorphous area.

Vickers hardness was measured to be 180 ± 3Hv in as-annealed wire; by cold drawing, the value increased to 471 ± 12Hv (52% reduction) and 463 ± 8Hv (62% reduction). These values were lower than those obtained for binary TiNi after the similar drawing reduction (535Hv in 51% reduction and 554Hv in 58% reduction). More detailed investigation on the mechanical properties of the drawn wires is underway.

4. Conclusions

It was shown that the amorphous/nanocrystalline hybrid wires of TiNi can be successfully produced by severe cold drawing. The processed wires exhibit unique properties such as high Young's modulus, high-tensile strength, and large linear elastic recovery. It was also confirmed that the drawing over 62% can produce amorphous phase in Ti-41Ni-8.5Cu, which has never been reported before. These amorphous/nanocrystalline hybrid wires of TiNi have a high potential as materials for medical devices and actuators.

References

1. J. Koike and D.M. Parkin, Crystal-to-Amorphous Transformation of NiTi Induced by Cold Rolling, *J. Mater. Res.*, 1990, **5**, p 1414–1418
2. Y.V. Tat'yanin, V.G. Kurduymov, and V.B. Fedorov, Preparation of Ti-Ni Amorphous Alloy by Shear Deformation Under Pressure, *Phys. Met. Metallogr.*, 1986, **62**, p 133–137
3. H. Nakayama, K. Tsuchiya, Z.-G. Liu, M. Umemoto, K. Morii, and K. Shimizu, Process of Nanocrystallization and Partial Amorphization by Cold Rolling, *Mater. Trans.*, 2001, **42**, p 1987–1993
4. T. Waitz, K. Tsuchiya, T. Antretter, and F.D. Fischer, Phase Transformations of Nanocrystalline Martensitic Materials, *MRS Bull.*, 2009, **34**, p 814–821
5. K. Tsuchiya, M. Ohnuma, K. Nakajima, T. Koike, Y. Hada, Y. Todaka, and M. Umemoto, Materials Research Society, MRS, V1201–V1212
6. K. Tsuchiya, Y. Hada, T. Koyano, K. Nakajima, M. Ohnuma, T. Koike, Y. Todaka, and M. Umemoto, Production of TiNi Amorphous/Nanocrystalline Wire With High Strength and Elastic Modulus by Severe Cold Drawing, *Scr. Mater.*, 2009, **60**, p 749–752
7. M. Peterlechner, T. Waitz, and H.P. Karnthaler, Nanocrystallization of NiTi Shape Memory Alloys Made Amorphous by High-Pressure Torsion, *Scr. Mater.*, 2008, **59**, p 566–569
8. Y. Liu and H. Xiang, Apparent Modulus of Elasticity of Near-Equiatomic NiTi, *J. Alloys Compd.*, 1998, **270**, p 154–159
9. A. Gyobu, Y. Kawamura, T. Saburi, and H. Horikawa, *PRICM 3*, TMS, p 2719–2724
10. P.L. Rossiter, *The Electrical Resistivity of Metals and Alloys*, Cambridge University Press, Cambridge, 1987
11. T. Kakeshita, T. Fukuda, H. Tetsukawa, T. Saburi, K. Kindo, T. Takeuchi, M. Honda, S. Endo, T. Taniguchi, and Y. Miyako, Negative Temperature Coefficient of Electrical Resistivity in B2-Type Ti-Ni Alloys, *Jpn. J. Appl. Phys.*, 1998, **37**, p 2535–2539
12. S. Kanemaki, M. Suzuki, Y. Yamada, and U. Mizutani, Low Temperature Specific Heat, Magnetic Susceptibility and Electrical Resistivity Measurements in Ni-Ti Metallic Glasses, *J. Phys. F*, 1998, **18**, p 105–112
13. Y.F. Zheng, B.M. Huang, J.X. Zhang, and L.C. Zhao, The Microstructure and Linear Superelasticity of Cold-Drawn TiNi Alloy, *Mater. Sci. Eng. A*, 2000, **279**, p 25–35